ADVANCED ENERGY MATERIALS
www.advenergymat.de

Polysiloxane-Based Single-Ion Conducting Polymer Blend Electrolyte Comprising Small-Molecule Organic Carbonates for High-Energy and High-Power Lithium-Metal Batteries

Hai-Peng Liang, Maider Zarrabeitia, Zhen Chen, Sven Jovanovic, Steffen Merz, Josef Granwehr, Stefano Passerini, and Dominic Bresser**

Single-ion conducting polymer electrolytes are considered particularly attractive for realizing high-performance solid-state lithium-metal batteries. Herein, a polysiloxane-based single-ion conductor (PSiO) is investigated. The synthesis is performed via a simple thiol-ene reaction, yielding flexible and self-standing polymer electrolyte membranes (PSiOM) when blended with poly(vinylidene fluoride-*co*-hexafluoropropylene) (PVdF-HFP). When incorporating 57 wt% of organic carbonates, these polymer membranes provide a Li^+ conductivity of >0.4 mS cm^{-1} at 20 °C and a wide electrochemical stability window of more than 4.8 V. This excellent electrochemical stability allows for the highly reversible cycling of symmetric Li||Li cells as well as high-energy Li||$LiNi_{0.6}Mn_{0.2}Co_{0.2}O_2$ (NMC_{622}) and Li||$LiNi_{0.8}Mn_{0.1}Co_{0.1}O_2$ (NMC_{811}) cells for several hundred cycles at relatively high discharge and charge rates. Remarkably, Li||NMC_{811} cells with high mass loading cathodes provide more than 76% capacity retention at a high current density of 1.44 mA cm^{-2}, thus rendering this polymer electrolyte suitable for high-performance battery applications.

1. Introduction

Lithium-ion batteries (LIBs) are the state-of-the-art electrochemical energy storage technology for portable electronic devices and electric vehicles.[1–4] To achieve even higher energy densities, the use of lithium metal as the negative electrode is considered the next big step. However, the continuous electrolyte decomposition at the electrode|electrolyte interface, owing to the lack of a stable solid electrolyte interphase (SEI), results in low Coulombic efficiency (CE) and, potentially, dendritic lithium deposition. Thus eventually cause rapid cell failure and, in a worst case, accidental short-circuiting, posing severe safety issues and hindering commercialization.[5–7] Nonetheless, there has been a revitalized interest in lithium-metal anodes, encouraged by recent advances towards the stabilization of the anode|electrolyte interface. These advances were achieved by different strategies, including the formulation of beneficial electrolyte compositions,[8] the application of artificial interphases,[9] the use of 3D host matrices,[10] and the replacement of conventional liquid electrolytes by solid-state electrolytes.[11] Among these strategies, the utilization of solid-state electrolytes – inorganic and/or polymeric – potentially provides great advantages concerning the safe operation of lithium-metal anodes.[12,13]

The first report on polymer electrolytes, characterized by high flexibility and light weight, dated back to the late 1970s with poly(ethylene oxide) (PEO) serving as the lithium salt dissolving medium.[14,15] Later, gel-type polymer electrolytes were developed by swelling a polymer matrix, such as poly(vinylidene fluoride-*co*-hexafluoropropylene) (PVdF-HFP), polyacrylonitrile (PAN), or poly(vinyl alcohol) (PVA) with a lithium salt-containing liquid electrolyte.[16] In such systems, the polymer essentially takes over the role of the separator and is not actively involved in the charge transport. Differently, the lithium salt anions substantially contribute to the charge transport, resulting in a lithium transference number (t_{Li^+}) well below 0.5. This leads to a large concentration gradient and reversed electric field in the cell, which in turn results in large overpotentials, limited dis-/charge rates, and fast dendrite growth.[17–20] Accordingly, increasing the t_{Li^+}, ideally to a value close to unity, provides a solution to overcome the above mentioned challenges. The most straightforward approach to realize this is the covalent tethering of the anionic function to the polymer to immobilize the negative charge, yielding single-ion

H.-P. Liang, M. Zarrabeitia, Z. Chen, S. Passerini, D. Bresser
Helmholtz Institute Ulm (HIU)
Helmholtzstrasse 11, 89081 Ulm, Germany
E-mail: stefano.passerini@kit.edu; dominic.bresser@kit.edu
H.-P. Liang, M. Zarrabeitia, Z. Chen, S. Passerini, D. Bresser
Karlsruhe Institute of Technology (KIT)
P.O. Box 3640, 76021 Karlsruhe, Germany
S. Jovanovic, S. Merz, J. Granwehr
IEK-9
Forschungszentrum Jülich
Wilhelm-Johnen Straße
52425 Jülich, Germany
S. Jovanovic, J. Granwehr
Institute of Technical and Macromolecular Chemistry
RWTH Aachen University
52074 Aachen, Germany
The ORCID identification number(s) for the author(s) of this article can be found under https://doi.org/10.1002/aenm.202200013.

DOI: 10.1002/aenm.202200013

conducting polymer electrolytes (SIPEs). SIPEs, however, commonly suffer low ionic conductivities. Therefore, tremendous efforts have been made to improve the conductivity such as the modification of the anion chemistry,[21] the design of nanostructured ion-conducting channels,[22–24] and the realization of tailored polymer architectures to realize faster dynamics.[25] The current densities reported for the application in battery cells, however, rarely exceeds 0.5 mA cm^{-2}, which is still insufficient for practical use.[26] Another major limitation with regard to the widespread implementation of polymer electrolytes concerns the commonly limited stability towards oxidation, especially the frequently involved ether-type functional group, preventing the combination with high-energy cathode materials such as lithium nickel manganese cobalt oxide (NMC).[27]

The use of silicon-based polymers such as polysiloxane-type materials instead of carbon-based polymers has received rather little attention so far, despite their extensive use, e.g., in the coating industry owing to their excellent adhesion strength, outstanding thermal stability, and chemical inertness.[28] Recently, polysiloxanes were studied as protective coatings for lithium-metal electrodes, revealing suppressed dendrite growth due to their unique viscoelastic properties and the formation of stable interphases.[29–32] Moreover, it has been reported that conformal polysiloxane coatings alleviate side reactions at the interface between $LiNi_{0.6}Mn_{0.2}Co_{0.2}O_2$ (NMC_{622}) and $LiNi_{0.80}Co_{0.15}Al_{0.05}O_2$ (NCA) cathodes and the electrolyte or moisture, yielding an enhanced cycle life.[33,34] Polysiloxanes typically possess a low glass transition temperature (T_g), which commonly leads to an increased segmental motion, thus, potentially favoring charge transport. Nevertheless, only a few attempts have been made to synthesize polysiloxane-based SIPEs[35–39] and the employed hydrosilylation reaction requires the use of a platinum catalyst which is very costly and, therefore, renders the commercial scale-up very challenging.

Herein, we report the synthesis of a polysiloxane-based single-ion conductor (PSiO) via a high-yield thiol-ene reaction. We blended the PSiO with PVdF-HFP to obtain free-standing polymer electrolyte membranes (PSiOM) that show a suitable uptake of organic carbonates to support charge transport. As a result, this SIPE provides high Li^+ conductivities at ambient and elevated temperatures, shows very stable cycling of Li‖NMC_{622} and Li‖NMC_{811} cells, and allows for the application of extremely high current densities up to 7.2 mA cm^{-1}.

2. Results and Discussion

The lithiated PSiO ionomer was synthesized via a cost-effective one-step thiol-ene click-polymerization between the thiol groups of poly[(mercaptopropyl)methylsiloxane] (PMMS) and the vinyl group of lithium (3-methacryloyloxypropylsulfonyl) (trifluoromethylsulfonyl)imide (LiMTFSI) using 2,2-azobis(2-methylpropionitrile) (AIBN) as the initiator (**Figure 1**a). The analysis by Fourier-transform infrared (FT-IR) spectroscopy, displayed in Figure 1b, reveals that the characteristic vibration peaks of the C = C double bond ($\bar{\nu}$ = 1634 cm^{-1}; LiMTFSI) and the −SH thiol group ($\bar{\nu}$ = 2557 cm^{-1}; PMMS) are not observed anymore in the FT-IR spectrum recorded for PSiO. The complete reaction of the two educts is further corroborated by ^{1}H NMR spectroscopy (Figure S1, Supporting Information), as the two proton peaks at 6.04 and 5.68 ppm, ascribed to the vinyl group in LiMTFSI, are not present anymore in the PSiO

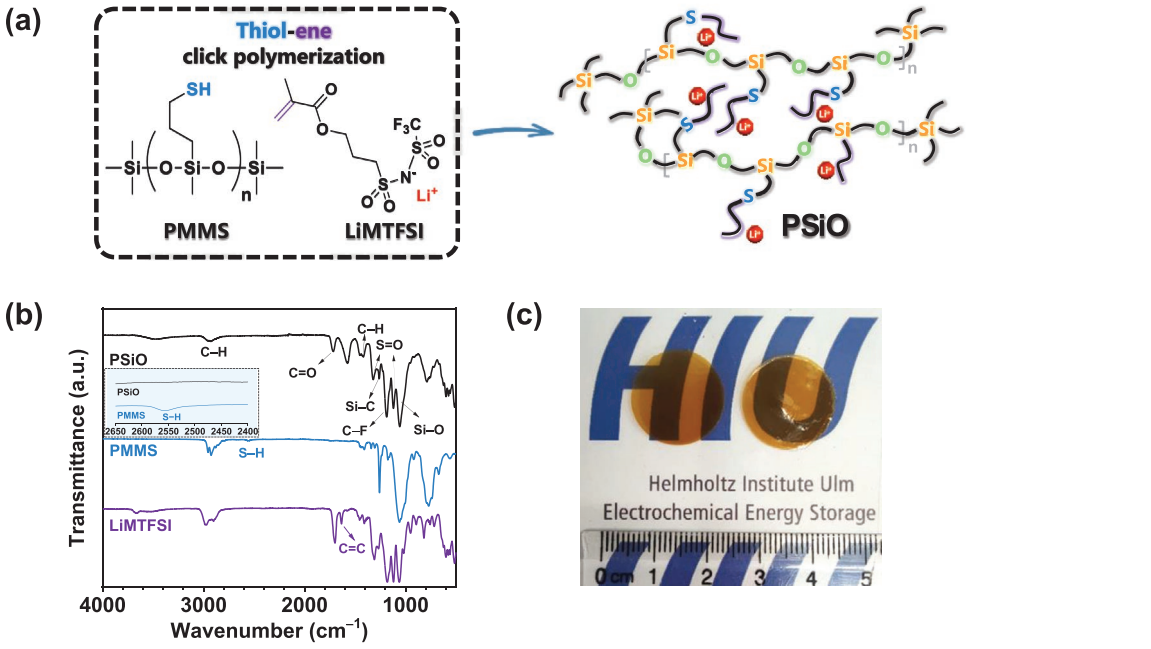

Figure 1. a) Schematic illustration of the PSiO synthesis via thiol-ene click polymerization. b) FT-IR spectra of the two educts LiMTFSI (bottom, in purple) and PMMS (middle, in blue) as well as PSiO (top, in black) as the final product; the inset shows a magnification of the region from 2650 to 2400 cm^{-1} where the signal of the thiol group disappears upon polymerization. c) Photograph of the blended PSiO+PVdF-HFP (PSiOM) electrolyte membranes.

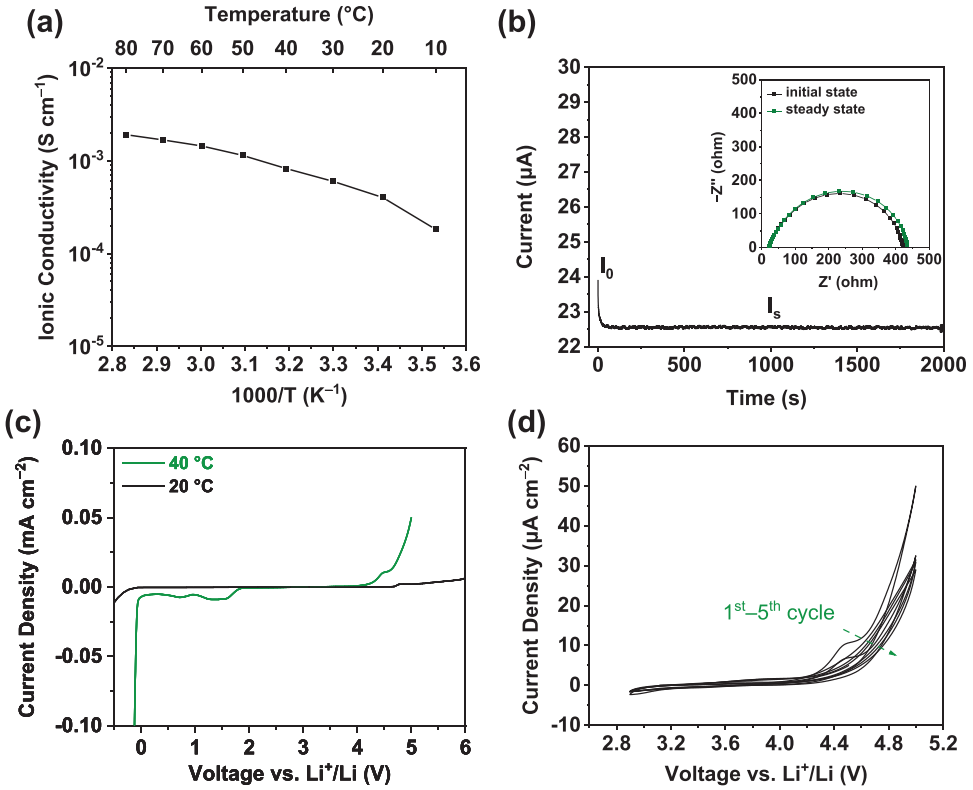

Figure 2. a) Temperature-dependent ionic conductivity of the PSiOM electrolyte. b) Electrochemical determination of t_{Li^+} by combining a chronoamperometry experiment (DC voltage: 10 mV) with EIS (inset) for Li‖Li cells. The initial current I_0 and the steady-state current I_s are indicated in the figure. c) Determination of the electrochemical stability window in Li‖SS (stainless steel) cells at 20 °C (in black) and 40 °C (in green) by LSV. d) CV experiment using the same cell setup conducted from OCV to 5.0 V for the first cyclic sweep and within a voltage range from 2.9 to 5.0 V for the subsequent cycles (T = 40 °C).

spectrum. The FT-IR spectrum of PSiO (Figure 1b) moreover shows the expected bands for the alkane C-H groups centered at $\overline{\nu}$ = 2926 and 1420 cm^{-1} and the polysiloxane backbone with the vibration bands at $\overline{\nu}$ = 1264 (Si–C) and 1054 cm^{-1} (Si–O).[40] The structural features of the anionic trifluoromethanesulfonylimide group are evident at $\overline{\nu}$ = 1326 and 1114 cm^{-1} for the S = O bond and at 1187 cm^{-1} for the C-F bond.[41,42] Following this confirmation of the complete reaction of the two educts, the PSiO ionomer was blended with PVdF-HFP to yield self-standing polymer electrolyte membranes (PSiOM; Figure 1c) with a thickness of about 45 ± 5 µm (Figure S2, Supporting Information) and high thermal stability exceeding 240 °C (Figure S3, Supporting Information).

The temperature-dependent ionic conductivity of the self-standing PSiOM electrolyte membranes (see Video S1 in the Supporting Information) comprising a mixture of organic carbonates (EC/DEC/FEC at a volume ratio of 48.8:48.8:2.4) was studied in a temperature range from 10 to 80 °C (**Figure 2**a). The conductivity plot shows a Vogel–Tammann–Fulcher (VTF) behavior, suggesting that the Li^+ transport is related to the segmental motion of PSiO, specifically the anionic side chains, and the mobility of the organic carbonate molecules, which are expected to support the Li^+ transfer from one side chain to another by acting simultaneously as "molecular transporter," additional coordination site, and plasticizing agent.[43,44] Generally, PSiOM reveals a remarkably high ionic conductivity with, e.g., 0.41 mS cm^{-1} at 20 °C, 0.60 mS cm^{-1} at 30 °C, and 0.82 mS cm^{-1} at 40 °C. Such a high conductivity is accompanied by high limiting current densities (J_{lim}), i.e., around 1.10 and 1.48 mA cm^{-2} at 20 and 40 °C, respectively (Figure S4, Supporting Information). The Li^+ transference number (t_{Li^+}) was determined by the Evans–Vincent–Bruce method (Figure 2b),[45] providing a value of 0.96, which underlines that essentially only the lithium cations contribute to the ionic conductivity measured.

To gain additional insights into the charge transport complementary to the Evans–Vincent–Bruce method for the determination of t_{Li^+}, the lithium and fluorine diffusion coefficients in PSiOM were determined by ^{7}Li and ^{19}F pulsed field gradient NMR (PFG-NMR) spectroscopy. The experiments were performed for PSiOM comprising either a mixture of EC and DEC or a mixture of EC, DEC, and FEC in order to exclude any potential impact of the FEC. A single, well-defined lithium diffusion component was observed with essentially identical diffusion coefficients for both solvent mixtures, i.e., 1.14 (±0.08) × 10^{-10} m^2 s^{-1} for EC/DEC and 1.19 (±0.07) × 10^{-10} m^2 s^{-1} for EC/DEC/FEC. The arithmetic mean of the relaxation mode obtained by Laplace inversion analysis provided the same result (Figure S5a, Supporting Information). For the ^{19}F resonance of the anion –CF_3 group, however, three different modes of mobility were observed (Figure S5b, Supporting Information): a fast, narrow diffusion component, centered at 2.8 × 10^{-10} m^2 s^{-1} with an integral of

about 39% of the total signal, a slower component centered at 8.5×10^{-12} m^2 s^{-1} with an integral of about 6% of the total signal, and a bias that represents an immobile species with an intensity of 55% of the total signal. The uncertainty of the diffusion coefficient from the width of the mode amounts to about one third of a decade. The random error of the integral is below 1%, but systematic errors are likely to underestimate the bias component. The observation of a fast fluorine species with a diffusion coefficient of the same order of magnitude as the one determined for lithium in combination with the findings obtained by the Evans–Vincent–Bruce method suggests a more complex charge transport mechanism. One explanation consistent with the data would be that LiMTFSI did not quantitatively react with the thiol groups of PMMS, but that the synthesis partially yielded relatively smaller molecules with saturated vinyl groups such as dimers or small oligomers, which are rather mobile in the swollen membranes. This explanation is supported by the finding that no variation of the -CF_3 chemical shift was observed between the mobile and the immobile fraction of the ^{19}F diffusion signal of the trifluoromethylsulfonyl group. Such globally neutral species do not significantly add to the net charge transport, but they might contribute to the Li^+ mobility,[46,47] especially as the exchange rates with the polymerized species (i.e., the immobile fluorine species) might be fast, while the ^7Li and the mobile ^{19}F species show a very similar diffusion coefficient. Such contribution to the overall lithium mobility might, for instance, include the support of the Li^+ transfer between PSiO side chains – comparable to the Li^+ coordinating organic carbonate molecules. Therefore, the combined presence of both the polymer-immobilized anions and the mobile anionic groups may add to the high ionic conductivity of the PSiO membrane, with the former being responsible for the overall charge transport and the latter for a reduction of energy barriers of translational motion. Additionally, more in-depth analyses of the different species and their contribution to the charge transport are currently carried out in our labs and will be reported in a follow-up manuscript.

Next, the electrochemical stability of the PSiOM electrolyte was investigated by linear sweep voltammetry (LSV) and cyclic voltammetry (CV). At 20 °C the current response is rather flat with a slight upturn at about 4.8 V upon oxidation (Figure 2c), which might be related to the oxidation of DMSO traces,[23,48] EC,[49] or the polymer itself. Indeed, there is a continuous, slightly increasing current flow at further elevated potentials, indicating that there is a continuous oxidative process occurring. When increasing the temperature to 40 °C, there is a stepwise increase in current density observed, starting at about 4.5 V. This initial anodic current shoulder might be as well related to DMSO traces.[23,48] In fact, this shoulder is observed only in the first scan when conducting CV experiments in the elevated potential range, but disappears in the following sweeps (Figure 2d). Nonetheless, beyond 4.6 V there is a steady increase in current density, revealing that the anodic stability of PSiOM is limited to this value at 40 °C. For the LSV toward reduction (Figure 2c), a similar behavior is observed: At 20 °C the current response is very flat until 0 V, when the onset of lithium plating occurs. Differently, at 40 °C some broad reduction peaks were detected, starting from about 1.8 V with a maximum at ≈1.4 V, which are ascribed to the reduction of EC, DEC, and residual DMSO traces.[50,51] This assignment is further supported by the observation that this broad feature at rather high voltages vanishes after the first reduction sweep when conducting CV experiments in the given voltage range (Figure S6, Supporting Information).

The compatibility with lithium-metal electrodes was further studied by performing lithium stripping and plating in symmetric Li|PSiOM|Li cells (**Figure 3**a). The cells exhibit an essentially constant overpotential of about 70 mV throughout the whole experiment for more than 550 h without any apparent increase or fluctuation, demonstrating a very good compatibility of the PSiOM electrolyte with lithium metal and an excellent interfacial stability. The cells were subsequently disassembled in an argon-filled glove box to conduct ex situ scanning electron microscopy (SEM) analysis of the cycled lithium foils.

A comparison of the pristine and cycled lithium electrodes is shown in Figure 3b,c, respectively. The cycled lithium electrode reveals a remarkably smooth surface without any indication of mossy or dendritic lithium growth despite a total capacity of 67.5 mAh cm^{-2} that was cycled in the preceding stripping and plating experiment. Moreover, also when applying varying current densities, ranging from 0.1 to 0.5 mA cm^{-2}, a very stable overpotential is observed that is as small as 26 mV at 0.1 mA cm^{-2} and increases only very slowly to 51 mV at 0.2 mA cm^{-2}, 73 mV at 0.3 mA cm^{-2}, 94 mV at 0.4 mA cm^{-2}, and 114 mV at 0.5 mA cm^{-2} (Figure 3d). These values are considerably smaller than those that have been reported for other SIPEs[52,53] or composite polymer electrolytes.[54] Furthermore, the critical current density was determined to be 0.9 mA cm^{-2} (Figure S7, Supporting Information), exceeding the values reported earlier for many state-of-the-art solid electrolytes.[26] Besides, the constant voltage response shown in Figure 3e underlines the findings concerning $t_{Li^+} \approx 1$, i.e., the absence of any appreciable reversed polarization at such current density.

To scrutinize the surface chemistry of the cycled lithium electrodes an ex situ X-ray photoelectron spectroscopy (XPS) analysis was performed—before (indicated as 0 min) and after Ar^+ sputtering for 20 min (**Figure 4**). In a first step, the ex situ XPS results obtained prior to the Ar^+ sputtering (0 min) are discussed. In the high-resolution C 1s photoelectron line (Figure 4a), five peaks are observed at 284.8, 286.7, 288.2, 289.4, and 290.4 eV, which correspond to C–H/C–C (hydrocarbons), C–O–C/–CH_2 (ethers/PVdF), –COOR (ester), –CO_3/CF_2 (carbonates/PVdF), and –CF_x bonds/groups, respectively.[55,56] The carbon–oxygen species are mainly originating from the reduction of the carbonate solvents, while the presence of –CH_2 and –CF_2 is assigned to PVdF-HFP. The O 1s spectrum (Figure 4b) shows the chemical species that have been observed also in the C 1s region (i.e., –C = O, –C–O–C–, and –COOR), a very minor fraction of Li_2O at 528.3 eV. This is presumably part of the native passivation layer, but might also be formed along the reductive decomposition of the oxygen-containing electrolyte components, as well as –S = O and –Si–O at 532.0 eV.[55,57] The latter two indicate that PSiO-related species are contributing to the interphase formation. The F 1s spectrum (Figure 4c) shows two distinct peaks at 688.0 and 685.0 eV, which are ascribed to –CF_x and LiF, respectively. These two species are assigned to the contribution of PVdF-HFP, FEC, and/or PSiO and their decomposition/dehydrofluorination products.[58,59] The presence of LiF is confirmed in the Li 1s spectrum (Figure 4d). Additionally,

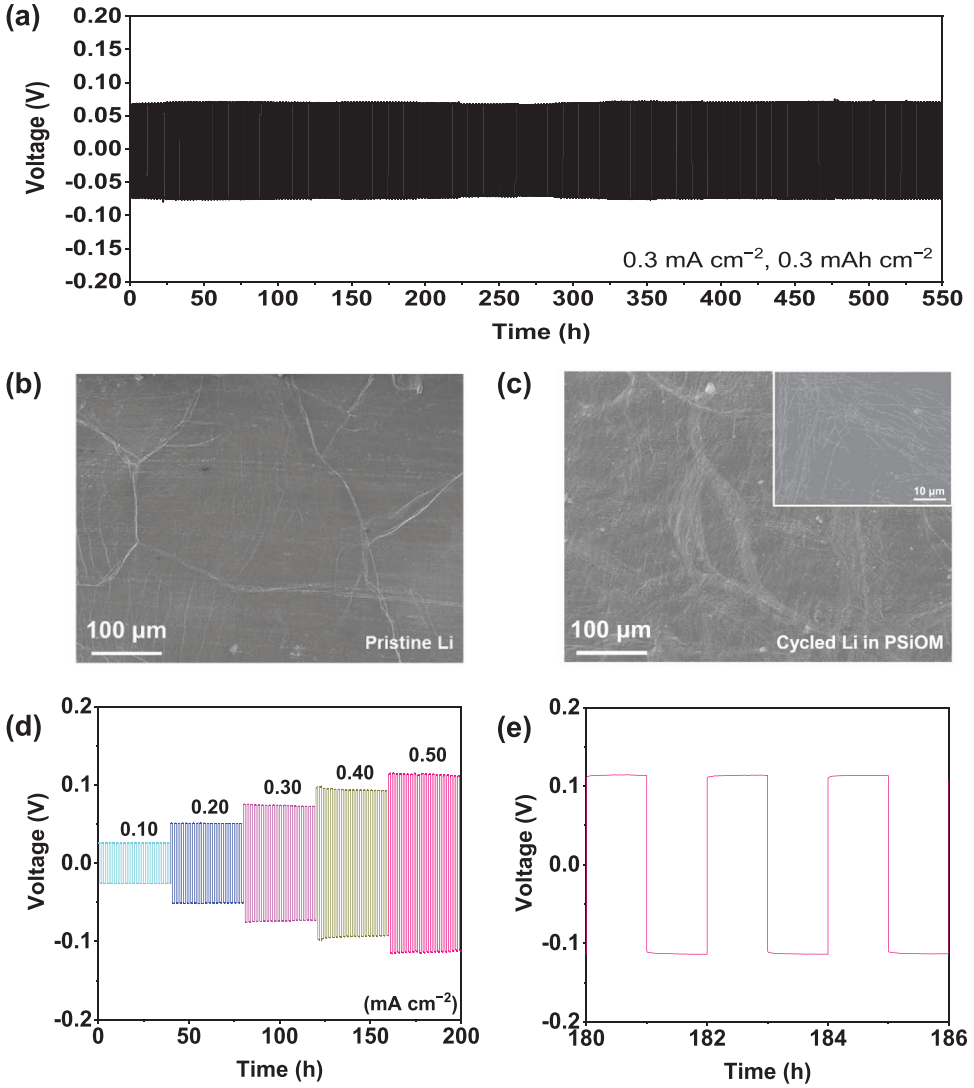

Figure 3. a) Lithium stripping and plating experiment via galvanostatic cycling of Li|PSiOM|Li cells, applying a current density of 0.3 mA cm^{-2} for 1 h (each step), i.e., cycling a total capacity of 0.3 mAh cm^{-2}. b,c) SEM micrographs of the b) pristine and c) cycled lithium foil; a magnification of the latter is provided as inset. d) Lithium stripping and plating experiment via galvanostatic cycling of Li|PSiOM|Li cells, applying varying current densities and e) a magnification of representative stripping and plating cycles at 0.5 mA cm^{-2}.

the peak at 57.8 eV might indicate the contribution of the LiMTFSI side chain (–LiMTFSI) to the SEI. Further peaks at 55.0 eV and 53.1 eV are attributed to Li_2CO_3/Li_xSiO_y and Li_2O, respectively. Just like Li_2O, Li_2CO_3 might be part of the native passivation layer, as the lithium foil is processed under an Ar/CO_2 atmosphere,[60] while it is also a common product of the reductive decomposition of organic carbonates at the lithium surface.[6] The finding of Li_xSiO_y further corroborates the contribution of PSiO to the interphase formation. The presence of –LiMTFSI is moreover confirmed by the S 2p photoelectron line (Figure 4e), which also shows RSO– and C–S species.[61] Finally, in the Si 2p region (Figure 4f), two major peaks are observed, which are ascribed to Si–O/Li_xSiO_y (102.4 eV) and Si–CH_3 (101.8 eV)[55] as reaction products of PSiO upon reduction at the lithium-metal electrode.

In a second step, the ex situ XPS results, obtained after 20 min Ar^+ sputtering, are discussed. Upon surface etching, the intensities related to the decomposition products of EC, DEC, and FEC (i.e., –C–O–C– and –COOR) in the C 1s and O 1s spectra decrease (note that lithium carbonate is also part of the native passivation layer). Simultaneously, a new peak at 283.8 eV appears, which is ascribed to –Si–CH_3. This finding suggests that the inner SEI layer is increasingly composed of PSiO-related species. Besides, the changes in the O 1s, F 1s, Li 1s, and S 2p spectra shows an increased concentration of inorganic electrolyte decomposition species such as Li_2O, LiOH, LiF, Li_2S, and Li_xSiO_y, which is in line with previous studies suggesting an inorganic species dominated SEI layer close to the lithium metal surface.[6,9,62] Generally, such layered SEI structure was found to be advantageous for the stabilization of the Li|electrolyte interface. The presence of LiF, Li_2O, and Li_2S, for instance, yields to low electronic conductivity, suppressing the decomposition of the organic carbonates combined with relatively low diffusion barrier for the lithium cations.[6,63–66]

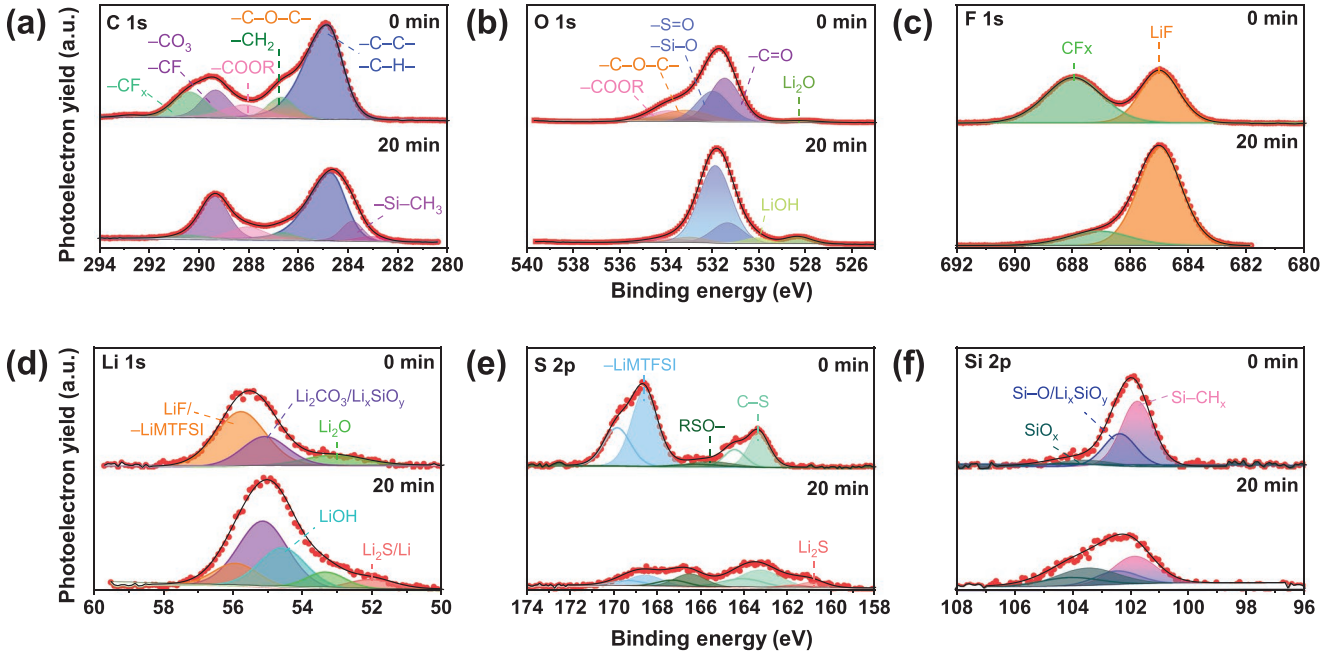

Figure 4. Ex situ XPS analysis of lithium electrodes subjected to lithium stripping and plating cycles for 550 h (see also Figure 3a) before (indicated as 0 min) and after 20 min of Ar^+ sputtering (sputtering rate of 0.8 nm min^{-1}): a) C 1s, b) O 1s, c) F 1s, d) Li 1s, e) S 2p, and f) Si 2p.

The presence of Li_xSiO_y (resulting from a polydimethylsiloxane-based protective layer) was found to support maintaining the integrity of the SEI.[29,30] In sum, the given composition of the SEI appears very beneficial for the realization of a stable SEI at the lithium-metal electrode, favoring the homogeneous and dense lithium deposition.

Following these highly motivating results, we investigated the potential combination of the PSiOM electrolyte with high-energy Ni-rich cathode materials. First, we assembled Li|PSiOM|NMC_{622} cells and subjected these to CV experiments and galvanostatic cycling (**Figure 5**). The CV curves (Figure 5a) show the typical redox couple associated with the reversible phase transition from a hexagonal to a monoclinic phase (H1→M).[67] It appears noteworthy that current response is very flat towards the anodic reversing voltage and that there is no significant increase in current density observed upon cycling. This indicates that PSiOM is sufficiently stable towards delithiated NMC_{622}. Figure 5b displays the comparative evaluation of the rate capability of Li|PSiOM|NMC_{622} cells at 20 and 40 °C. Here, 1C is defined as 180 mA g^{-1} (equivalent to a current density of 0.41 mA cm^{-2} considering the average active material mass loading of ≈2.3 mg cm^{-2}), which means that the applied dis-/charge rates of 0.1C, 0.3C, 0.5C, 2C, 3C, 4C, and 5C correspond to current densities of 0.04, 0.12, 0.21, 0.82, 1.23, 1.64, and 2.05 mA cm^{-2}, respectively. A detailed overview of the average specific capacities at different C rates and temperatures is provided in Table S1.

Expectedly, the specific capacity across all C rates is higher at 40 °C – with, e.g., 177 mAh g^{-1} at 0.1C, 155 mAh g^{-1} at 1C, and remarkable 123 mAh g^{-1} at 5C – owing to the higher ionic conductivity of the PSiOM electrolyte and generally faster charge transport and diffusion. This is also reflected in the higher polarization when comparing the corresponding dis-/charge profiles, especially at elevated C rates (Figure S8). The long-term cycling stability was examined as well at both temperatures and varying C rates, i.e., at 0.5C and 1C for T = 20 °C (Figure 5c) as well as at 1C and 2C for T = 40 °C (Figure 5d). In all cases, the Li|PSiOM|NMC_{622} cells reveal an excellent cycling stability for more than 500 cycles, and the detailed capacities are presented in Table S2. At 0.5C and 20 °C, the capacity retention is as high as 90% and the average CE is 99.6%. When increasing the C rate to 1C at the same temperature, the capacity retention decreases slightly to 88%, while the CE increases to 99.8%, indicating that the reduced time at elevated potentials might be beneficial for the CE. When increasing the temperature to 40 °C, the capacity retention for the 1C cycling remains essentially the same with 87% and the same is true for the average CE with 99.8%, while the specific capacity is generally higher, as observed beforehand for the rate capability test. Even when cycling the cell at a rather high C rate of 2C, the capacity retention is still as high as 80% after 500 cycles.

With regard to this outstanding cycling stability, we studied in a second step the suitability of PSiOM in combination with NMC_{811} cathodes and subjected these to CV experiments and galvanostatic cycling as well (**Figure 6**). In Figure 6a, the CV data are presented, revealing the typical redox features for the reversible H1→M, M→H2, and H2→H3 phase transitions.[48] The results for the rate capability tests at 20 and 40 °C are depicted in Figure 6b. In this case, a dis-/charge rate of 1C is defined as 200 mA g^{-1} (equivalent to a current density of 0.46 mA cm^{-2} considering the average active material mass loading of ≈2.3 mg cm^{-2}), which means that the applied dis-/charge rates of 0.1C, 0.3C, 0.5C, 2C, 3C, 4C, and 5C correspond to current densities of 0.05, 0.14, 0.23, 0.92, 1.38, 1.84, and 2.30 mA cm^{-2}, respectively. The same trend as for the Li|PSiOM|NMC_{622} cells is observed, i.e., the specific capacity

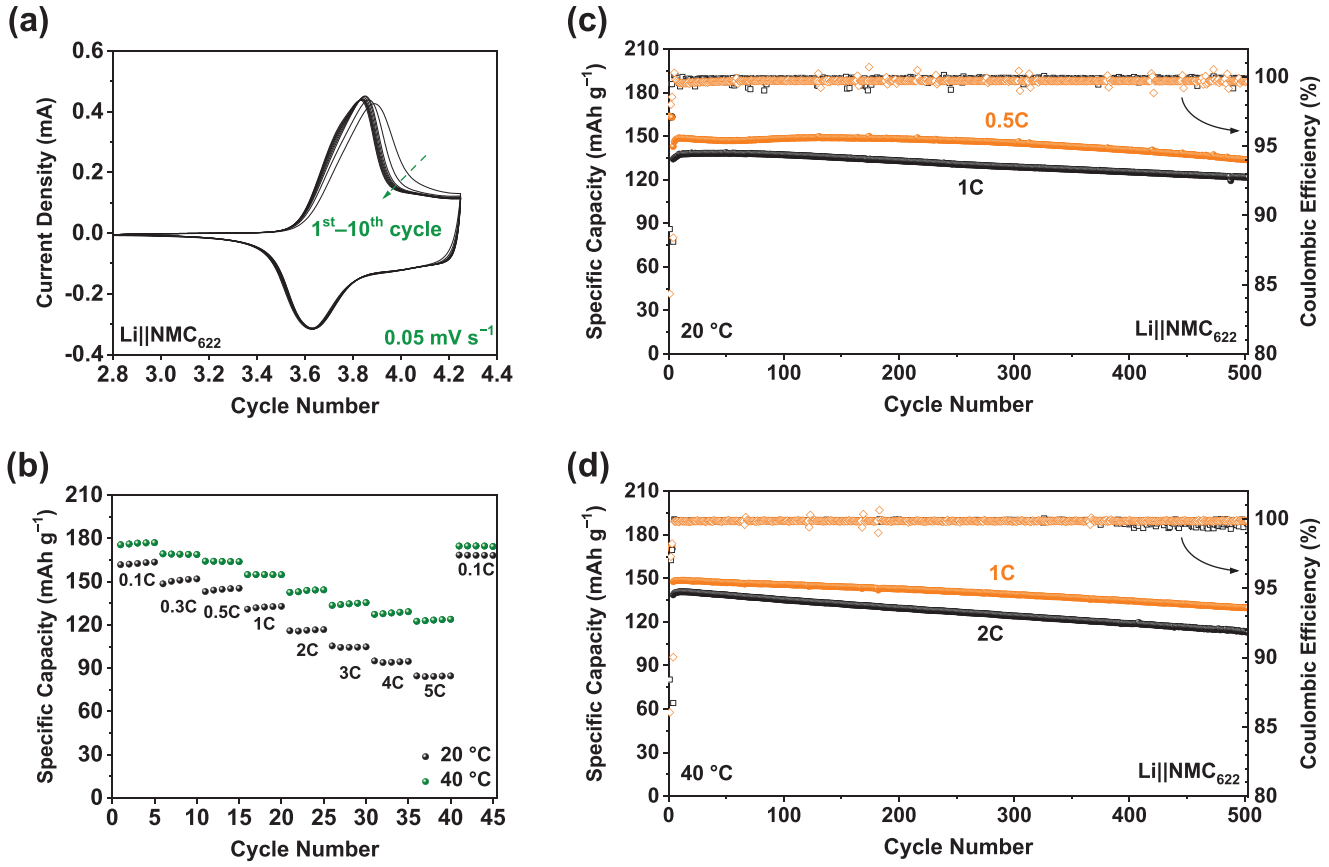

Figure 5. Electrochemical characterization of Li|PSiOM|NMC_{622} cells (cut-off/reversing voltages: 2.8 and 4.25 V): a) CV experiment for 10 cyclic sweeps with a sweep rate of 0.05 mV s^{-1} at 40 °C; b) galvanostatic cycling and application of varying C rates from 0.1C to 5C and back to 0.1C at 20 °C (in black) and at 40 °C (in green); c) constant current cycling at 20 °C with a C rate of 0.5C (in orange) and 1C (in black) after three formation cycles at 0.1C; d) constant current cycling at 40 °C with a C rate of 1C (in orange) and 2C (in black) after three formation cycles at 0.1C.

is substantially higher at 40 °C, particularly at elevated C rates, due to the lower polarization (Figure S9, Supporting Information). A detailed overview of all average specific capacity values is included in Table S1 (Supporting Information). For instance, at 0.1C and 40 °C, the Li|PSiOM|NMC_{811} cells provide a specific capacity of 195 mAh g^{-1}, which slightly decreases to 165 mAh g^{-1} at 1C and 130 mAh g^{-1} at 5C, highlighting the excellent performance of PSiOM. In addition, these cells can be cycled stably for several hundred cycles with a remarkable capacity retention of 92% at 0.5C and 84% at 1C at 20 °C after 300 cycles owing to the high average CE of about 99.9% (Figure 6c). At 40 °C and 1C the capacity retention is even higher with 90% and decreases only little to 86% at 2C (Figure 6d). A detailed overview of the evolution of the specific capacity is provided in Table S2 (Supporting Information).

To further foster the applicability of PSiOM in practical cells, we eventually increased the NMC_{811} active material mass loading from about 2.3 mg cm^{-2} to 7.2 mg cm^{-2}. This increase in mass loading comes with a trice increase of the current density applied at a given C rate, which has been rarely investigated in lithium polymer batteries. The rate capability tests for these high-mass loading Li|PSiOM|NMC_{811} cells is presented in **Figure 7**a—once again at 20 and 40 °C. When applying rather low current densities (i.e., 0.14 mA cm^{-2}), the cells provide specific capacities of 184 and 198 mAh g^{-1} at 20 and 40 °C, respectively, and more than 71% (T = 20 °C) and 76% (T = 40 °C) of this specific capacity is retained when then current density is increased by one order of magnitude (i.e., 1.44 mA cm^{-2}). A detailed overview of the capacity retention as a function of the current density applied is provided in Figure S10 (Supporting Information). In brief, when increasing the current density (T = 40 °C), the capacity gradually decreases to, e.g., 170 mAh g^{-1} at 0.72 mA cm^{-2}, 151 mAh g^{-1} at 1.44 mA cm^{-2} and 125 mAh g^{-1} at 2.88 mA cm^{-2}, while still showing decent capacities at current densities as high as 5.76 and 7.20 mA cm^{-2}, far exceeding the limiting current density. While this is presumably reflected in the slight decrease upon cycling at such high current densities, it still shows that PSiOM can generally withstand very high peak currents, as also confirmed by the fact that the capacity almost increases back to the same values as before when decreasing the current density again at the end of the rate capability test. Figure 7b displays the constant current cycling at 1.44 mA cm^{-2} of Li||NMC_{811} cells comprising PSiOM in comparison with Li||NMC_{811} cells containing a liquid electrolyte (1 M $LiPF_6$ in EC/DEC (V/V = 1/1) with 2.4 V% FEC; the non-normalized capacity plots are shown in Figure S11 in the Supporting Information). It is immediately apparent that the Li|PSiOM|NMC_{811} cell greatly outperforms the Li||NMC_{811} cell comprising the

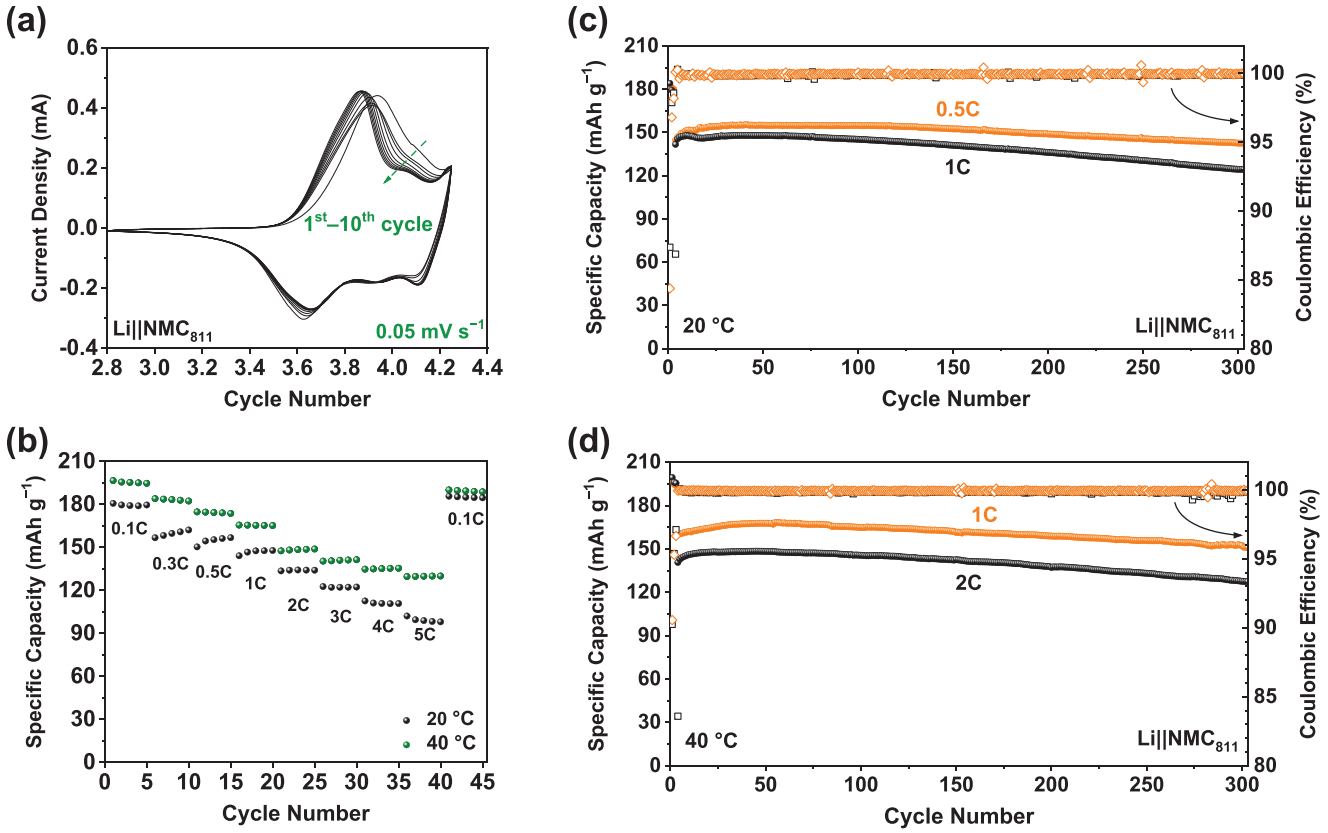

Figure 6. Electrochemical characterization of Li|PSiOM|NMC_{811} cells (cut-off/reversing voltages: 2.8 and 4.25 V): a) CV experiment for 10 cyclic sweeps with a sweep rate of 0.05 mV s^{-1} at 40 °C; b) galvanostatic cycling and application of varying C rates from 0.1C to 5C and back to 0.1C at 20 °C (in black) and at 40 °C (in green); c) constant current cycling at 20 °C with a C rate of 0.5C (in orange) and 1C (in black) after three formation cycles at 0.1C; d) constant current cycling at 40 °C with a C rate of 1C (in orange) and 2C (in black) after three formation cycles at 0.1C.

liquid electrolyte in terms of cycling stability with a capacity retention of about 80% after 150 cycles compared to only 30% in the case of the liquid electrolyte. A quick check by initially replenishing the liquid electrolyte does not lead to any increase in capacity after the cell fade. However, the subsequent replacement of the lithium anode results in a regain of the initial capacity values (Figure S12, Supporting Information), revealing that the origin for this poor capacity retention is the lithium electrode—or, more specifically, the interface of the lithium electrode with the liquid electrolyte. As a matter of fact, the lithium electrode cycled with the liquid electrolyte shows large cracks and a very rough/needle-like surface (Figure 7c). Differently, the lithium electrode cycled with PSiOM shows a relatively smooth and crack-free surface (Figure 7d). The ex situ SEM analysis of the cross-section further supports the much more favorable lithium deposition in the case of PSiOM. For the liquid electrolyte (Figure 7e), the remaining bulk lithium has a thickness of about 350 µm while the surface layer has a large thickness of around 140 µm. This surface layer appears moreover very rough and rather porous. In stark contrast, the bulk lithium in the case of the PSiOM-containing Li||NMC_{811} cell remains much thicker (about 400 µm) while the surface film is substantially thinner (≈90 µm) and denser (Figure 7f). These findings indicate that the single-ion conducting PSiOM electrolyte allows for a more uniform Li^+ flux across a stabilized lithium|electrolyte interface (and interphase), resulting in a smooth lithium deposition and stable cycling of Li||NMC_{811} cells at commercially relevant current densities of more than 1 mA cm^{-2}. We may briefly note here that the composition of the liquid electrolyte, resembling the composition of the organic carbonates incorporated in the PSiOM membranes, might not be ideal for lithium-metal batteries. We chose $LiPF_6$ as the conducting salt to avoid any potential anodic dissolution reaction of the aluminum current collector, while other salt compositions and concentrations might be more favorable, indeed. Nonetheless, to the best of our knowledge, these results are at least among the best so far reported for (quasi-)solid-state polymer-based electrolytes in Li||NMC battery cells, as summarized in Table S3.

3. Conclusions

A polysiloxane-based single-ion conductor (PSiO) was synthesized via a facile one-step thiol-ene reaction, yielding self-standing and flexible polymer electrolyte membranes (PSiOM) when blended with PVdF-HFP. The incorporation of small-molecule organic carbonates (57 wt%) allows for a high Li^+ conductivity, e.g., >0.4 mS cm^{-1} at 20 °C and >0.8 mS cm^{-1} at 40 °C. This PSiOM electrolyte shows highly stable cycling of lithium

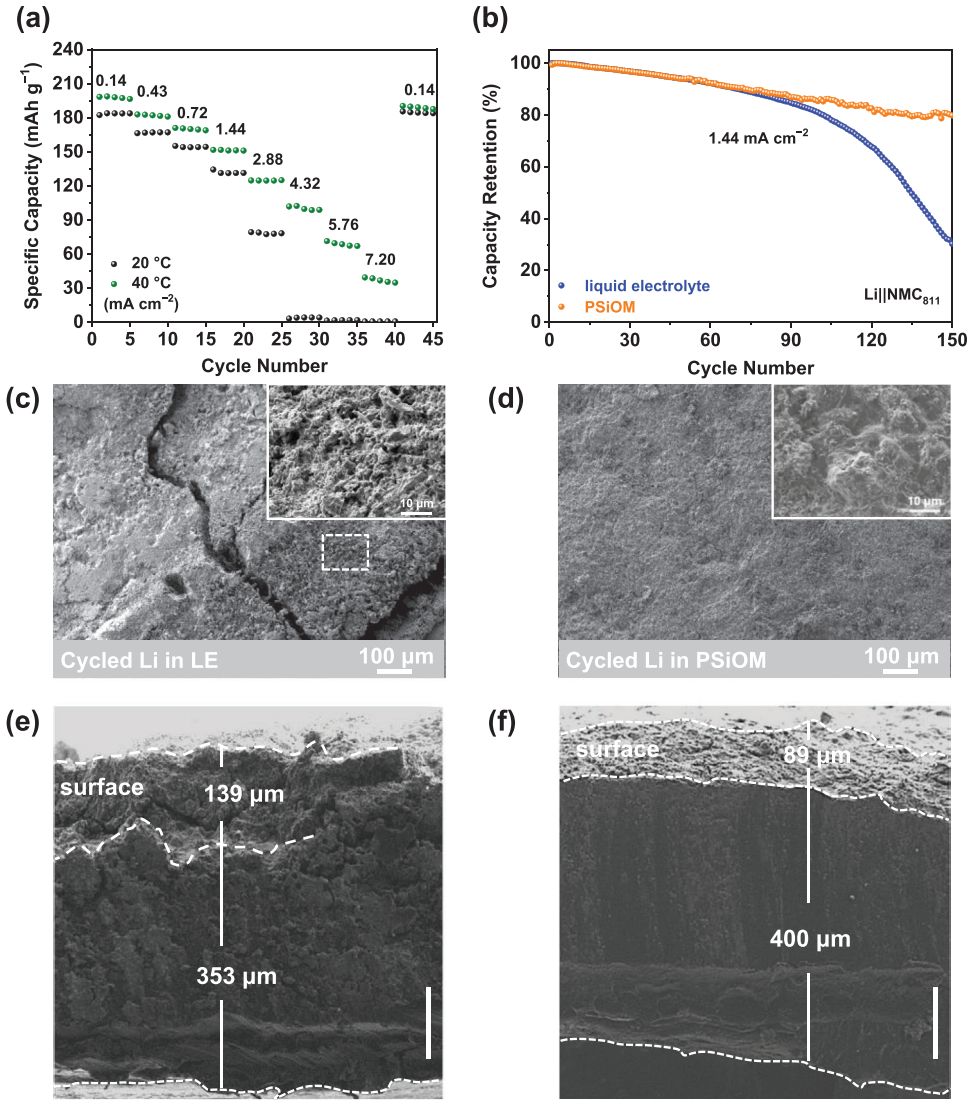

Figure 7. a) Rate capability test of high-mass loading Li|PSiOM|NMC$_{811}$ cells at varying current densities with T = 20 °C (in black) and T = 40 °C (in green); cut-off voltages: 2.8 and 4.25 V. b) Comparison of the constant current cycling of Li||NMC$_{811}$ cells comprising the PSiOM electrolyte (in orange) or a liquid electrolyte (LE; in blue) with an applied current density of 1.44 mA cm^{-2} at 40 °C (after three formation cycles at 0.14 mA cm^{-2}, not shown herein; the specific capacity was normalized for the sake of comparability). c–f) Ex situ SEM analysis of the cycled lithium electrodes from b) with a view at c,d) the surface and e,f) the cross-section for c,e) the liquid electrolyte and d,f) PSiOM; insets in c,d) provide a magnification of the lithium electrode surface and the scale bar in the lower right in e,f) refers to 100 µm.

metal electrodes and, moreover, high-energy Li||NMC$_{622}$ and Li||NMC$_{811}$ cells for several hundred cycles at 20 and 40 °C owing to its wide electrochemical stability window. Remarkably, high-mass loading Li|PSiOM|NMC$_{811}$ cells outperform Li||NMC$_{811}$ cells comprising a liquid organic carbonate-based electrolyte at a high current density of 1.44 mA cm^{-2}. These results underline the great potential of well-designed single-ion conducting polymer electrolytes for high-energy and high-power lithium-metal batteries.

4. Experimental Section

Synthesis of the PSiO Ionomer and Preparation of the PSiOM Electrolyte Membranes: Lithium (3-methacryloyloxypropylsulfonyl)(trifluoromethylsulfonyl)imide (LiMTFSI) was synthesized according to a previous study.[42] Subsequently, LiMTFSI (3.36 g, 9.75 mmol), 1.31 g poly[(mercaptopropyl)methylsiloxane] (PMMS, SMS-992, M_w = 4000–7000, 75–150 cSt, Gelest), and 66 mg 2,2-azobis(2-methylpropionitrile) (AIBN, purified through recrystallization before use) were dissolved in 20 mL anhydrous tetrahydrofuran (THF) in a Schlenk flask. The above mixture was stirred under argon at 65 °C for 12 h to complete the polymerization (Scheme S1, Supporting Information). Afterward the solvent was removed via rotary evaporation. Following a repeated reprecipitation in acetone/dichloromethane, an amber oil was obtained. The subsequent drying under vacuum provided the solid PSiO ionomer (yield 81%).

The polymer electrolyte membranes (PSiOMs) were prepared by solvent casting. 0.275 g PSiO and 0.225 g poly(vinylidene fluoride-*co*-hexafluoropropylene) (PVdF-HFP) were dissolved in a 1:4 volume mixture of acetone and dimethyl sulfoxide (DMSO) at room temperature. The solvent was evaporated at 80 °C, followed by vacuum drying at 80 °C for

2 days to provide a brownish membrane (PSiOM, 45 ± 5 µm thickness). From the thus obtained membranes round discs with a diameter of 12 mm were punched out and soaked for 48 h with a mixture of organic carbonates, i.e., ethylene carbonate (EC), diethyl carbonate (DEC), and fluoroethylene carbonate (FEC) in a volume ratio of 48.8:48.8:2.4. The solvent uptake was calculated by the weight difference before and after swelling, revealing an average uptake of 130 wt% with regard to the mass of the dry membrane, which corresponds to 57 wt% of the total mass of the final electrolyte membranes.

Physicochemical Characterization: ^{1}H NMR spectra were collected on a Bruker DMX400 NMR spectrometer. Fourier-transform infrared (FT-IR) spectra were collected on a Spectrum Two spectrometer (Perkin-Elmer) in an attenuated total reflectance (ATR) mode. Thermogravimetric analysis (TGA) was conducted on a Netzsch TG 209 F1 at a heating rate of 10 K min^{-1} under N_2/O_2 (V/V = 1:1) atmosphere. Scanning electron microscopy (SEM) was performed using a Supra 55 field-emission scanning electron microscope (Zeiss). The samples were transferred to the microscope utilizing a hermetic shuttle box to avoid any contact to the ambient atmosphere. Cycled lithium electrodes were analyzed also by means of X-ray photoelectron spectroscopy (XPS). Prior to the analysis the cycled electrodes were rinsed with dimethyl carbonate, dried at room temperature in the glove box, and transferred to the XPS using a hermetic argon-filled vessel. XPS analysis was conducted via a Phoibos 150 spectrometer equipped with a monochromatic Al-Kα (1486.6 eV) X-ray source. The scans were acquired at 200 W with a pass energy of 20 eV and a step-size of 0.1 eV in a fixed analyzer transmission mode. Depth profiling was performed with a focused ion gun (5 keV, Ar^+) and an ion filter for 20 min (≈0.8 nm min^{-1}). The binding energies were calibrated with regard to the C 1s carbon peak at 285 eV.[55,68] The lithium and fluorine self-diffusion coefficients were determined via ^{7}Li and ^{19}F pulsed-field gradient NMR (PFG-NMR) spectroscopy. Samples of PSiOM swollen in EC/DEC (V:V = 1/1) and EC/DEC/FEC ($V/V/V$ = 48.8/48.8/2.4) were prepared in 5 mm NMR tubes. PFG-NMR spectroscopy was conducted on a Bruker Avance III HD spectrometer with a 9.4 T wide-bore magnet and a broadband gradient probe with diffusion capabilities (Bruker DiffBB) at a temperature of 40 °C. PFG stimulated echo (STE) sequences with bipolar pulses were employed in order to suppress eddy currents arising in the conductive material due to the switching magnetic field gradients. The experimental parameters are provided in Table S4 (Supporting Information). The ^{7}Li diffusion coefficient D_{Li}^{NMR} was determined by fitting the experimental data to the Stejskal–Tanner equation

$$S(b) = S_0 \cdot e^{-bD_{Li}^{NMR}} \tag{1}$$

with

$$b = \gamma^2 G^2 \delta^2 \left(\Delta - \frac{\delta}{3}\right) \tag{2}$$

$S(b)$ is the signal intensity, S_0 the signal intensity for $b = 0$, γ the gyromagnetic ratio of the observed nucleus, G the magnetic field gradient strength, δ the gradient duration, and Δ the diffusional mixing time. Only a single diffusion component was observed for the ^{7}Li PFG experiments. For the ^{19}F PFG experiments, the distribution of diffusion coefficients was determined by means of an inverse Laplace transform (ILT). The same procedure and parametrization was followed as described in a previous study.[69]

Electrode Preparation: For the electrode preparation, 90 wt% $LiNi_{0.6}Mn_{0.2}Co_{0.2}O_2$ (NMC_{622}, BASF) or $LiNi_{0.8}Mn_{0.1}Co_{0.1}O_2$ (NMC_{811}, BASF), 2 wt% PVdF (Solvay), 4 wt% PSiO, and 4 wt% conductive carbon (Super C_{65}, Imerys) were dispersed in a suitable amount of *n*-methyl-2-pyrrolidone (NMP, >99.5%, Sigma-Aldrich). The resulting slurry was cast on aluminum foil (battery grade) using the doctor-blade technique. After drying at 80 °C for 2 h, round discs with a diameter of 12 mm were punched from the electrode sheets and dried under vacuum at 100 °C for 12 h. The electrodes for the tests with the liquid electrolyte had the following composition: 92 wt% active material, 4 wt% PVdF, and 4 wt% conductive carbon. The electrodes were prepared analogously to the electrodes used for the investigation of the PSiOM electrolyte. The electrodes were pressed at 10 t cm^{-2} before cell assembly. The active material mass loading was 2.3 ± 0.1 mg cm^{-2}, resulting in an electrode coating thickness of about 10 µm for the pressed electrodes. Additionally, NMC_{811} electrodes with a higher active material mass loading of ≈7.2 mg cm^{-2} were prepared following the same procedure, having an electrode coating thickness of around 23 µm after pressing.

Electrochemical Characterization: For the determination of the ionic conductivity (σ), the PSiOM electrolyte membranes were sandwiched between two copper electrodes in a vacuum-sealed pouch cell. The cell assembly was conducted in the dry room with a dew point of less than −65 °C. The ionic conductivity was determined by evaluating the bulk resistance obtained via electrochemical impedance spectroscopy (EIS), conducted on a Solartron SI 1260 in a frequency range from 100 kHz to 100 mHz with a voltage amplitude of 10 mV. The temperature ranged from 10 to 80 with 10 °C steps. The cells were kept at each temperature for 2 h in a climatic chamber (Binder) to stabilize prior to the EIS measurement. The impedance spectra were fitted and analyzed using the RelaxIS software (rhd instruments). The ionic conductivity was calculated using the following equation

$$\sigma = \frac{d}{RS} \tag{3}$$

with d being the thickness of the electrolyte membrane, R the bulk resistance, and S the electrode surface area. The Li^+ transference number (t_{Li^+}) was determined via the Bruce–Vincent–Evans method.[45] The PSiOM electrolyte membranes were sandwiched between two lithium electrodes (Φ = 14 mm) in coin cells (CR2032, Hohsen). The impedance spectra were collected in a frequency range from 100 kHz to 100 mHz with a 10 mV AC voltage. t_{Li^+} was calculated via the following equation

$$t_{Li^+} = \frac{I_s(\Delta V - I_0 R_0)}{I_0(\Delta V - I_s R_s)} \tag{4}$$

with ΔV being the DC voltage, I_0 and I_s the current in the initial and steady state, respectively, as well as R_0 and R_s the resistance in the initial and steady state, respectively.

The electrochemical stability of the polymer electrolyte was investigated by linear sweep voltammetry (LSV; sweep rate 1 mV s^{-1}) and cyclic voltammetry (CV; sweep rate 0.1 mV s^{-1}) on a Biologic VMP3 using a stainless steel disc as working electrode and lithium metal (500 µm, battery grade, Honjo) as counter and reference electrode. The J_{lim} was determined by performing LSV with a sweep rate of 0.02 mV s^{-1} at 40 °C. Lithium stripping and plating experiments were performed in symmetric Li‖Li coin cells at 40 °C. The same temperature was applied for the CV experiments for the Li‖NMC cells in a voltage range from 2.8 to 4.25 V versus Li^+/Li with a sweep rate of 0.05 mV s^{-1}. Galvanostatic cycling of the Li‖NMC_{622} (1C = 180 mA g^{-1}) and Li‖NMC_{811} (1C = 200 mA g^{-1}) coin cells was conducted in the same voltage range using a Maccor 4000 battery testing device. The liquid electrolyte used for comparison was 1 M $LiPF_6$ in EC/DEC (V/V = 1/1) with 2.4 V% FEC. All cells were assembled in an argon-filled glove box with a H_2O and O_2 content of less than 0.1 ppm.

Supporting Information

Supporting Information is available from the Wiley Online Library or from the author.

Acknowledgements

The authors would like to acknowledge financial support from the Federal Ministry of Education and Research (BMBF) within the

FestBatt project (03XP0175B and 13XP0176B) and from the Helmholtz Association. Moreover, the authors would like to thank R.-A. Eichel (FZ Jülich) for helpful discussions.

Open access funding enabled and organized by Projekt DEAL.

Conflict of Interest

The authors declare no conflict of interest.

Data Availability Statement

The data that support the findings of this study are available on request from the corresponding author. The data are not publicly available due to privacy or ethical restrictions.

Keywords

electrolytes, lithium batteries, polymers, polysiloxane, single-ion conductors

Received: January 3, 2022
Revised: February 27, 2022
Published online:

[1] M. Li, J. Lu, Z. Chen, K. Amine, *Adv. Mater.* **2018**, *30*, 1800561.
[2] M. Armand, P. Axmann, D. Bresser, M. Copley, K. Edström, C. Ekberg, D. Guyomard, B. Lestriez, P. Novák, M. Petranikova, W. Porcher, S. Trabesinger, M. Wohlfahrt-Mehrens, H. Zhang, *J. Power Sources* **2020**, *479*, 228708.
[3] D. Bresser, K. Hosoi, D. Howell, H. Li, H. Zeisel, K. Amine, S. Passerini, *J. Power Sources* **2018**, *382*, 176.
[4] M. Marinaro, D. Bresser, E. Beyer, P. Faguy, K. Hosoi, H. Li, J. Sakovica, K. Amine, M. Wohlfahrt-Mehrens, S. Passerini, *J. Power Sources* **2020**, *459*, 228073.
[5] A. Yoshino, *Angew. Chem., Int. Ed.* **2012**, *51*, 5798.
[6] X. He, D. Bresser, S. Passerini, F. Baakes, U. Krewer, J. Lopez, C. T. Mallia, Y. Shao-Horn, I. Cekic-Laskovic, S. Wiemers-Meyer, F. A. Soto, V. Ponce, J. M. Seminario, P. B. Balbuena, H. Jia, W. Xu, Y. Xu, C. Wang, B. Horstmann, R. Amine, C.-C. Su, J. Shi, K. Amine, M. Winter, A. Latz, R. Kostecki, *Nat. Rev. Mater.* **2021**, *6*, 1036.
[7] B. Horstmann, J. Shi, R. Amine, M. Werres, X. He, H. Jia, F. Hausen, I. Cekic-Laskovic, S. Wiemers-Meyer, J. Lopez, D. Galvez-Aranda, F. Baakes, D. Bresser, C.-C. Su, Y. Xu, W. Xu, P. Jakes, R.-A. Eichel, E. Figgemeier, U. Krewer, J. M. Seminario, P. B. Balbuena, C. Wang, S. Passerini, Y. Shao-Horn, M. Winter, K. Amine, R. Kostecki, A. Latz, *Energy Environ. Sci.* **2021**, *14*, 5289.
[8] H. Yang, J. Li, Z. Sun, R. Fang, D.-W. Wang, K. He, H.-M. Cheng, F. Li, *Energy Storage Mater.* **2020**, *30*, 113.
[9] X.-B. Cheng, R. Zhang, C.-Z. Zhao, F. Wei, J.-G. Zhang, Q. Zhang, *Adv. Sci.* **2016**, *3*, 1500213.
[10] P. Shi, X.-Q. Zhang, X. Shen, R. Zhang, H. Liu, Q. Zhang, *Adv. Mater. Technol.* **2020**, *5*, 1900806.
[11] Y. Zheng, Y. Yao, J. Ou, M. Li, D. Luo, H. Dou, Z. Li, K. Amine, A. Yu, Z. Chen, *Chem. Soc. Rev.* **2020**, *49*, 8790.
[12] J. Kalhoff, G. G. Eshetu, D. Bresser, S. Passerini, *ChemSusChem* **2015**, *8*, 2154.
[13] A. Varzi, R. Raccichini, S. Passerini, B. Scrosati, *J. Mater. Chem. A* **2016**, *4*, 17251.
[14] D. E. Fenton, J. M. Parker, P. V. Wright, *Polymer* **1973**, *14*, 589.
[15] M. Armand, *Solid State Ion* **1994**, *69*, 309.
[16] F. Baskoro, H. Q. Wong, H.-J. Yen, *ACS Appl. Energy Mater.* **2019**, *2*, 3937.
[17] J.-N. Chazalviel, *Phys. Rev. A* **1990**, *42*, 7355.
[18] C. Brissot, M. Rosso, J.-N. Chazalviel, S. Lascaud, *J. Power Sources* **1999**, *81–82*, 925.
[19] K. M. Diederichsen, E. J. McShane, B. D. McCloskey, *ACS Energy Lett.* **2017**, *2*, 2563.
[20] M. Doyle, T. F. Fuller, J. Newman, *Electrochim. Acta* **1994**, *39*, 2073.
[21] H. Zhang, C. Li, M. Piszcz, E. Coya, T. Rojo, L. M. Rodriguez-Martinez, M. Armand, Z. Zhou, *Chem. Soc. Rev.* **2017**, *46*, 797.
[22] Y. Du, H. Yang, J. M. Whiteley, S. Wan, Y. Jin, S.-H. Lee, W. Zhang, *Angew. Chem., Int. Ed.* **2016**, *55*, 1737.
[23] H.-D. Nguyen, G.-T. Kim, J. Shi, E. Paillard, P. Judeinstein, S. Lyonnard, D. Bresser, C. Iojoiu, *Energy Environ. Sci.* **2018**, *11*, 3298.
[24] D. Bresser, M. Leclere, L. Bernard, P. Rannou, H. Mendil-Jakani, G.-T. Kim, T. Zinkevich, S. Indris, G. Gebel, S. Lyonnard, L. Picard, *ChemSusChem* **2021**, *14*, 655.
[25] J. Zhu, Z. Zhang, S. Zhao, A. S. Westover, I. Belharouak, P.-F. Cao, *Adv. Energy Mater.* **2021**, *11*, 2003836.
[26] Y. Lu, C. Zhao, H. Yuan, X. Cheng, J. Huang, Q. Zhang, *Adv. Funct. Mater.* **2021**, *31*, 2009925.
[27] M. Wetjen, G.-T. Kim, M. Joost, G. B. Appetecchi, M. Winter, S. Passerini, *J. Power Sources* **2014**, *246*, 846.
[28] Y. Abe, T. Gunji, *Prog. Polym. Sci.* **2004**, *29*, 149.
[29] J. Meng, F. Chu, J. Hu, C. Li, *Adv. Funct. Mater.* **2019**, *29*, 1902220.
[30] F. Liu, Q. Xiao, H. B. Wu, L. Shen, D. Xu, M. Cai, Y. Lu, *Adv. Energy Mater.* **2018**, *8*, 1701744.
[31] J. Lopez, A. Pei, J. Y. Oh, G.-J. N. Wang, Y. Cui, Z. Bao, *J. Am. Chem. Soc.* **2018**, *140*, 11735.
[32] B. Zhu, Y. Jin, X. Hu, Q. Zheng, S. Zhang, Q. Wang, J. Zhu, *Adv. Mater.* **2017**, *29*, 1603755.
[33] H. Wang, W. Ge, W. Li, F. Wang, W. Liu, M.-Z. Qu, G. Peng, *ACS Appl. Mater. Interfaces* **2016**, *8*, 18439.
[34] Z. Yang, Z. Li, Y. Huang, M. Zhang, C. Liu, D. Zhang, G. Cao, *J. Power Sources* **2020**, *471*, 228480.
[35] D. P. Siska, D. F. Shriver, *Chem. Mater.* **2001**, *13*, 4698.
[36] J. F. Snyder, J. C. Hutchison, M. A. Ratner, D. F. Shriver, *Chem. Mater.* **2003**, *15*, 4223.
[37] R. Rohan, K. Pareek, Z. Chen, W. Cai, Y. Zhang, G. Xu, Z. Gao, H. Cheng, *J. Mater. Chem. A* **2015**, *3*, 20267.
[38] Z. Zhang, J. Jin, F. Bautista, L. Lyons, N. Shariatzadeh, D. Sherlock, K. Amine, R. West, *Solid State Ion* **2004**, *170*, 233.
[39] U. H. Choi, S. Liang, M. V. O'Reilly, K. I. Winey, J. Runt, R. H. Colby, *Macromolecules* **2014**, *47*, 3145.
[40] K. Liu, A. Pei, H. R. Lee, B. Kong, N. Liu, D. Lin, Y. Liu, C. Liu, P. Hsu, Z. Bao, Y. Cui, *J. Am. Chem. Soc.* **2017**, *139*, 4815.
[41] L. Porcarelli, A. S. Shaplov, M. Salsamendi, J. R. Nair, Y. S. Vygodskii, D. Mecerreyes, C. Gerbaldi, *ACS Appl. Mater. Interfaces* **2016**, *8*, 10350.
[42] H.-P. Liang, Z. Chen, X. Dong, T. Zinkevich, S. Indris, S. Passerini, D. Bresser, *Macromol. Rapid Commun.* **2022**, 2100820.
[43] D. Bresser, S. Lyonnard, C. Iojoiu, L. Picard, S. Passerini, *Mol. Syst. Des. Eng.* **2019**, *4*, 779.
[44] S. B. Aziz, T. J. Woo, M. F. Z. Kadir, H. M. Ahmed, *J. Sci. Adv. Mater. Dev.* **2018**, *3*, 1.
[45] J. Evans, C. A. Vincent, P. G. Bruce, *Polymer* **1987**, *28*, 2324.
[46] P. S. Pregosin, *Prog. Nucl. Magn. Reson. Spectrosc.* **2006**, *49*, 261.
[47] S. Zugmann, M. Fleischmann, M. Amereller, R. M. Gschwind, H. D. Wiemhöfer, H. J. Gores, *Electrochim. Acta* **2011**, *56*, 3926.
[48] Z. Chen, D. Steinle, H.-D. Nguyen, J.-K. Kim, A. Mayer, J. Shi, E. Paillard, C. Iojoiu, S. Passerini, D. Bresser, *Nano Energy* **2020**, *77*, 105129.
[49] I. Azcarate, W. Yin, C. Méthivier, F. Ribot, C. Laberty-Robert, A. Grimaud, *J. Electrochem. Soc.* **2020**, *167*, 080530.
[50] X. Zhang, R. Kostecki, T. J. Richardson, J. K. Pugh, P. N. Ross, *J. Electrochem. Soc.* **2001**, *148*, A1341.

[51] Y. Yamada, Y. Takazawa, K. Miyazaki, T. Abe, *J. Phys. Chem. C* **2010**, *114*, 11680.
[52] C. Cao, Y. Li, Y. Feng, P. Long, H. An, C. Qin, J. Han, S. Li, W. Feng, *J. Mater. Chem. A* **2017**, *5*, 22519.
[53] C. Cao, Y. Li, S. Chen, C. Peng, Z. Li, L. Tang, Y. Feng, W. Feng, *ACS Appl. Mater. Interfaces* **2019**, *11*, 35683.
[54] H. Wang, Q. Wang, X. Cao, Y. He, K. Wu, J. Yang, H. Zhou, W. Liu, X. Sun, *Adv. Mater.* **2020**, *32*, 2001259.
[55] G. Beamson, *Science ESCA 300 Database* **1992**.
[56] R. I. R. Blyth, H. Buqa, F. P. Netzer, M. G. Ramsey, J. O. Besenhard, P. Golob, M. Winter, *Appl. Surf. Sci.* **2000**, *167*, 99.
[57] C. D. Wagner, W. M. Riggs, L. E. Davis, J. F. Moulder, G. E. Muilenberg, *Handbook of X-Ray: Photoelectron Spectroscopy*, Phys. Electron. Div., Eden Prairie Minn, xxxx **1979**, p. 55344.
[58] R. Crowe, J. P. S. Badyal, *J. Chem. Soc. Chem. Commun.* **1991**, *0*, 958.
[59] Y. Okuno, K. Ushirogata, K. Sodeyama, Y. Tateyama, *Phys. Chem. Chem. Phys.* **2016**, *18*, 8643.
[60] T. Fujieda, N. Yamamoto, K. Saito, T. Ishibashi, M. Honjo, S. Koike, N. Wakabayashi, S. Higuchi, *J. Power Sources* **1994**, *52*, 197.
[61] H. Kim, F. Wu, J. T. Lee, N. Nitta, H.-T. Lin, M. Oschatz, W. I. Cho, S. Kaskel, O. Borodin, G. Yushin, *Adv. Energy Mater.* **2015**, *5*, 1401792.
[62] Z. Chen, G.-T. Kim, J.-K. Kim, M. Zarrabeitia, M. Kuenzel, H.-P. Liang, D. Geiger, U. Kaiser, S. Passerini, *Adv. Energy Mater.* **2021**, *11*, 2101339.
[63] Q. Zhang, *Nat. Nanotechnol.* **2018**, *13*, 623.
[64] J. Tan, J. Matz, P. Dong, J. Shen, M. Ye, *Adv. Energy Mater.* **2021**, *11*, 2100046.
[65] B. Han, Z. Zhang, Y. Zou, K. Xu, G. Xu, H. Wang, H. Meng, Y. Deng, J. Li, M. Gu, *Adv. Mater.* **2021**, *33*, 2100404.
[66] G. M. Hobold, J. Lopez, R. Guo, N. Minafra, A. Banerjee, Y. Shirley Meng, Y. Shao-Horn, B. M. Gallant, *Nat. Energy* **2021**, *6*, 951.
[67] R. Jung, M. Metzger, F. Maglia, C. Stinner, H. A. Gasteiger, *J. Electrochem. Soc.* **2017**, *164*, A1361.
[68] C. Xu, B. Sun, T. Gustafsson, K. Edström, D. Brandell, M. Hahlin, *J. Mater. Chem. A* **2014**, *2*, 7256.
[69] S. Merz, P. Jakes, S. Taranenko, R.-A. Eichel, J. Granwehr, *Phys. Chem. Chem. Phys.* **2019**, *21*, 17018.